Bipartite and tripartite output entanglement in three-mode optomechanical systems

Ying-Dan Wang, Stefano Chesi, and Aashish A. Clerk

Phys. Rev. A **91**, 013807 — Published 5 January 2015

DOI: 10.1103/PhysRevA.91.013807

Bipartite and tripartite output entanglement in 3-mode optomechanical systems

Ying-Dan Wang,[1,2] Stefano Chesi,[3] and Aashish A. Clerk[2]

[1] *Institute of Theoretical Physics, Chinese Academy of Sciences, Beijing 100190, China*
[2] *Department of Physics, McGill University, 3600 rue University, Montreal, QC Canada H3A 2T8*
[3] *Beijing Computational Science Research Center, Beijing 100084, China*

We provide analytic insight into the generation of stationary itinerant photon entanglement in a 3-mode optomechanical system. We identify the parameter regime of maximal entanglement, and show that strong entanglement is possible even for weak many-photon optomechanical couplings. We also show that strong tripartite entanglement is generated between the photonic and phononic output fields; unlike the bipartite photon-photon entanglement, this tripartite entanglement diverges as one approaches the boundary of system stability.

PACS numbers: 42.50.Wk, 42.50.Ex, 07.10.Cm

I. INTRODUCTION

Entanglement is one of the most fascinating and potentially useful aspects of quantum systems. Of particular interest is the generation of entangled itinerant quanta (which can be easily spatially separated), and of true multipartite entanglement (involving irreducible correlations between three or more subsystems). These goals have been the subject of considerable theoretical and experimental work, in a variety of systems spanning quantum optics setups [1, 2], cold atoms [3], superconducting circuits [4–6] and spin qubits [7]. Optomechanical systems [8], where mechanical motion interacts with electromagnetic fields, could be another powerful platform to realize these goals. A key advantage here is the potential to use mechanical motion to entangle disparate subsystems (e.g., microwave and optical photons). A number of schemes to generate entangled photons in optomechanics have been studied theoretically [9–15]. Recent experiments have also demonstrated mechanically-mediated entanglement between two microwave pulses [16].

Here, we analyze theoretically both itinerant and multipartite entanglement in a 3-mode optomechanical system where two cavities are coupled to a single mode of a mechanical resonator. Such a setup has been realized in several recent experiments [17–19]. Previous theory work, largely numerical, examined bipartite output entanglement in this system [11, 13–15] but mostly focused on transient [15] or experimentally-challenging strong-coupling regimes [13, 14]. In contrast, we focus here on identifying optimal conditions to generate stationary output entanglement with *weak* many-photon optomechanical couplings. We obtain that maximum entanglement is achieved through a simple matching condition of optomechanical cooperativities. Surprisingly, this operation point coincides with the least favorable regime for the generation of intra-cavity entanglement. We provide a complete yet simple analytic understanding of the physics, which also allows us to illustrate the trade-off between large entanglement and thermal resilience, and uncover a sensitive dependence of entanglement on the time delay between emitted wave-packets.

We also address the generation of tripartite entanglement in such a hybrid 3-mode system, considering correlations between both output photons and phonons. While usually ignored, the mechanical output field could be accessed experimentally, using for example optomechanical crystal geometries with phonon waveguides [20], or by having the mechanical dissipation be dominated by a third auxiliary cavity used for cooling. We find that true hybrid tripartite entanglement is indeed created: the output state corresponds to a "twice-squeezed vacuum", involving two 2-mode squeezing operations. We also quantify this entanglement using the Gaussian Rényi-2 measure [21]. Besides being of fundamental interest, such tripartite entangled states have applications to a variety of quantum information processing tasks such as teleportation, tele-cloning, and dense coding [22, 23]. The present setup is especially suited to the continuous generation of non-local multipartite entanglement, as the phonons and photons from the two cavities are all emitted into spatially separated outputs. Note that Genes et al. [10] also studied tripartite entanglement in an optomechanical system, though in a setting where the entangled subsystems were not all spatially separated or itinerant.

It also worth noting that, while our emphasis here is on optomechanics, the physical features uncovered here apply generally to other bosonic 3-mode systems (e.g., realized with superconducting circuits [24, 25]).

Our paper is organized as follows: in Sec. II, we give the description of the physical system and its stability conditions. In Sec. III we obtain the optimal condition for bipartite output entanglement, based on an analytical solution. In Sec. IV, we analyze in detail various imperfections such as thermal noise, non-RWA corrections, internal losses, and finite bandwidth. In Sec. V, we describe how to achieve non-local tripartite output, which we quantify with the "residual Gaussian-Rényi-2" (GR2) entanglement measure. Section VI summarizes our results.

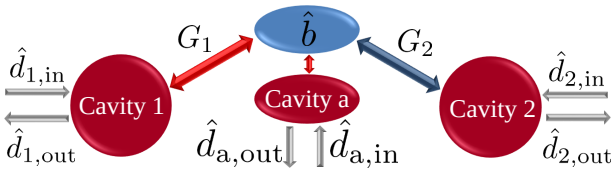

FIG. 1. System schematics. Two driven cavities (cavities 1 and 2) interact with a common mechanical resonator (mode $\hat{b}$). This can generate entanglement in the optical outputs. An auxiliary third cavity (cavity a) can be used to cavity cool the mechanics, and to make the mechanical output mode accessible.

II. PHYSICAL SYSTEM

We consider a 3-mode optomechanical system where two cavities are coupled to a single mode of a mechanical resonator (see Fig. 1). The standard optomechanical interacting Hamiltonian

$$\hat{H} = \omega_{\mathrm{m}}\hat{b}^{\dagger}\hat{b} + \sum_{i=1,2}\left[\omega_i\hat{a}_i^{\dagger}\hat{a}_i + g_i\left(\hat{b}^{\dagger}+\hat{b}\right)\hat{a}_i^{\dagger}\hat{a}_i\right] \qquad (1)$$

governs the system's dynamics, with $\hat{a}_i$ the annihilation operator for cavity i (frequency ω_i), $\hat{b}$ the annihilation operator of the mechanical mode (frequency ω_{m}), and g_i the optomechanical coupling strengths. In order to generate steady-state entanglement, cavity 1 (2) is driven at the red (blue) sideband associated with the mechanical resonator: $\omega_{d1} = \omega_1 - \omega_{\mathrm{m}}$ and $\omega_{d2} = \omega_2 + \omega_{\mathrm{m}}$. By working in an interaction picture with respect to the free Hamiltonian and following the usual linearization procedure [8], we have $\hat{H}^{\mathrm{R}} = \hat{H}_{\mathrm{int}} + \hat{H}_{\mathrm{CR}}(t)$ with

$$\hat{H}_{\mathrm{int}} = \left(G_1\hat{b}^{\dagger}\hat{d}_1 + G_2\hat{b}\hat{d}_2\right) + h.c. = \tilde{G}\left(\hat{b}^{\dagger}\hat{\beta}_A + h.c.\right), \qquad (2)$$

and $\hat{H}_{\mathrm{CR}}(t) = \tilde{G}\left(\hat{b}^{\dagger}\hat{\beta}_A^{\dagger}e^{2i\omega_{\mathrm{m}}t} + h.c.\right)$. Here $\hat{d}_i = \hat{a}_i - \bar{a}_i$ with $\bar{a}_i$ the classical cavity amplitude. $G_i = g_i\bar{a}_i$ is the dressed coupling (we take $g_i, \bar{a}_i > 0$ without loss of generality), $\tilde{G} = \sqrt{G_1^2 - G_2^2}$, and $\hat{\beta}_A = \hat{d}_1\cosh r + \hat{d}_2^{\dagger}\sinh r$ ($r = \tanh^{-1}(G_2/G_1)$) is a Bogoliubov mode.

We first focus on the resolved-sideband regime $\omega_{\mathrm{m}} \gg \kappa_1, \kappa_2$ and make the rotating wave approximation (RWA) by neglecting $\hat{H}_{\mathrm{CR}}$. The non-RWA corrections are treated in Sec. IV C. The combined swapping and entangling interactions in $\hat{H}_{\mathrm{int}}$ lead to a net entangling interaction between the two cavity modes; as discussed in [26], this interaction has a fundamentally dissipative nature. It is useful to diagonalize $\hat{H}_{\mathrm{int}}$ in terms of three normal modes [14, 26]: one "mechanically-dark" Bogoliubov mode $\hat{\beta}_B = \hat{d}_1\sinh r + \hat{d}_2^{\dagger}\cosh r$ (which is robust to mechanical thermal noise), and two coupled eigenmodes involving both the mechanics and cavities.

The dissipation of each mode is treated via standard input-output theory [27] and is given explicitly by the Langevin equations below:

$$\begin{aligned}
\frac{d}{dt}\hat{a} &= -\frac{\gamma}{2}\hat{a} - i\left(G_1\hat{d}_1 + G_2\hat{d}_2^{\dagger}\right) - \sqrt{\gamma}\hat{a}^{\mathrm{in}},\\
\frac{d}{dt}\hat{d}_1 &= -\frac{\kappa_1}{2}\hat{d}_1 - iG_1\hat{a} - \sqrt{\kappa_1}\hat{d}_1^{\mathrm{in}},\\
\frac{d}{dt}\hat{d}_2^{\dagger} &= -\frac{\kappa_2}{2}\hat{d}_2^{\dagger} + iG_2\hat{a} - \sqrt{\kappa_2}\hat{d}_2^{\mathrm{in},\dagger},
\end{aligned} \qquad (3)$$

where γ is the mechanical damping rate and $\kappa_{1,2}$ the external damping rates of the two cavities. We will first neglect the effect of internal damping rates $\kappa'_{1,2}$, discussed in detail in Sec. IV. In Eq. (3), $\hat{d}_j^{\mathrm{in}}$ are the input operators ($\hat{d}_{\mathrm{m}}^{\mathrm{in}} = \hat{a}^{\mathrm{in}}$) whose correlation functions are $\langle\hat{d}_j^{\mathrm{in}}(t)\hat{d}_k^{\mathrm{in},\dagger}(t')\rangle = N_j\delta(t-t')$. Here N_j is the average thermal population of each mode and, in the following discussion, we assume that the cavity thermal populations are always zero (due to the high frequency), while keeping the mechanical thermal population N_{m} finite.

The frequency-resolved output modes $\hat{d}_i^{\mathrm{out}}[\omega] \equiv \int d\omega e^{i\omega t}\hat{d}_i^{\mathrm{out}}(t)/\sqrt{2\pi}$ are related to the input by $\hat{d}_i^{\mathrm{out}}[\omega] = \sum_{j=1}^{3} S_{ij}[\omega]\hat{d}_j^{\mathrm{in}}[\omega]$ ($j = 3$ denotes the mechanical fields). The scattering matrix $\mathbf{S}[\omega]$ is obtained straightforwardly from the input-output relations $\hat{d}_i^{\mathrm{out}} = \sqrt{\kappa_i}\hat{d}_i + \hat{d}_i^{\mathrm{in}}$ [27] and the system Langevin equations (with RWA) as follows:

$$\mathbf{S}[\omega] = \mathbf{1} + \frac{1}{C_1\chi_1\chi_{\mathrm{m}} - C_2\chi_2\chi_{\mathrm{m}} + 1}\begin{pmatrix} \chi_1\left(\frac{C_2}{4}\chi_2\chi_{\mathrm{m}} - 1\right) & \frac{\sqrt{C_1C_2}}{4}\chi_1\chi_2\chi_{\mathrm{m}} & \frac{iC_1}{2}\chi_1\chi_{\mathrm{m}} \\ -\frac{\sqrt{C_1C_2}}{4}\chi_1\chi_2\chi_{\mathrm{m}} & -\chi_2\left(\frac{C_1}{4}\chi_1\chi_{\mathrm{m}} + 1\right) & -\frac{iC_2}{2}\chi_2\chi_{\mathrm{m}} \\ \frac{iC_1}{2}\chi_1\chi_{\mathrm{m}} & \frac{iC_2}{2}\chi_2\chi_{\mathrm{m}} & -\chi_{\mathrm{m}} \end{pmatrix}, \qquad (4)$$

with $\chi_i = 2\kappa_i/(\kappa_i - 2i\omega)$ ($i \in \{1, 2, \mathrm{m}\}$, $\kappa_{\mathrm{m}} \equiv \gamma$). Notice that at $\omega = 0$ the matrix only depends on the cooperativities.

Given the blue-detuned laser drive, a first question involves the stability of our linearized system. The Routh-Hurwitz conditions [28] yield two requirements [14, 26] to guarantee stability. The first is that $\gamma_{\mathrm{tot}} > 0$, where $\gamma_{\mathrm{tot}} = \gamma + 4G_1^2/\kappa_1 - 4G_2^2/\kappa_2$ is the effective damping rate of the mechanical resonator interacting with the two cavities. Focusing on the interesting and relevant regime of strong cooperativities $C_i \equiv 4G_i^2/(\gamma\kappa_i) \gg 1$ and $\kappa_i \gg \gamma$,

the two requirements can be combined into:

$$G_1^2/G_2^2 > \max(\kappa_2/\kappa_1, \kappa_1/\kappa_2). \quad (5)$$

III. BIPARTITE CAVITY OUTPUT ENTANGLEMENT

We start by discussing the entanglement of light leaving the two cavities. The following canonical mode operators:

$$\hat{D}_i^{\text{out}}[\omega, \sigma, \tau_i] = \frac{1}{\sqrt{\sigma}} \int_{\omega-\frac{\sigma}{2}}^{\omega+\frac{\sigma}{2}} d\omega' e^{-i\omega'\tau_i} \hat{d}_i^{\text{out}}[\omega']. \quad (6)$$

describe output temporal modes in a bandwidth σ centered about the frequency ω. τ_i sets the absolute time at which the wave packet of interest is emitted from cavity i; without loss of generality, we set $\tau_2 = 0$. The covariance matrix of the output operators can be computed via the scattering matrix. Then, the two-mode entanglement can be quantified using the logarithmic negativity $E_N^{\text{out}}[\omega, \sigma, \tau_1]$ [29, 30].

For clarity, we restrict ourselves in this section to the zero-bandwidth case $\sigma \to 0$; the result is then independent of τ_1 ($\hat{D}_i^{\text{out}}[\omega] \equiv \hat{D}_i^{\text{out}}[\omega, 0, \tau_i] e^{i\omega\tau_i}$, $E_N^{\text{out}}[\omega] \equiv E_N^{\text{out}}[\omega, 0, \tau_1]$). We first discuss a simple analytical solution of the bipartite cavity output entanglement and then derive the optimal condition for output entanglement. In the following section, we will relax the assumption of zero bandwidth σ. We will also discuss other possible imperfections and their influence on output entanglement: mechanical thermal noise, cavity internal losses, and non-RWA corrections.

A. Mapping to a two-mode squeezed thermal state

Using the standard approach (i.e. plugging the system covariance matrix into the definition of logarithmic negativity), the entanglement of the 3-mode system can be easily computed numerically. However, we find that mapping the output state to a 2-mode squeezed thermal state can yield a simple analytical expression which reveals a number of interesting properties of the output entanglement.

A 2-mode squeezed thermal state can be written as

$$\hat{\rho}_{12} = \hat{S}_{12}(R_{12}) \left[\hat{\rho}_1^{\text{th}}(\bar{n}_1) \otimes \hat{\rho}_2^{\text{th}}(\bar{n}_2)\right] \hat{S}_{12}^{\dagger}(R_{12}). \quad (7)$$

Here

$$\hat{S}_{12}(R_{12}) = \exp\left[R_{12}\hat{D}_1^{\text{out}}[0]\hat{D}_2^{\text{out}}[0] - h.c.\right] \quad (8)$$

is the two-mode squeeze operator, with R_{12} the squeezing parameter, and $\hat{\rho}_j^{\text{th}}(\bar{n}_j)$ describes a single-mode thermal state with average population $\bar{n}_j$. The output state is thus completely characterized by just 3 parameters: $\bar{n}_1$, $\bar{n}_2$ and R_{12} and the entanglement of this state (if $E_N^{\text{out}} \geq 0$) is simply given by:

$$E_N^{\text{out}} = -\ln\left(n_R - \sqrt{n_R^2 - (1+2\bar{n}_1)(1+2\bar{n}_2)}\right), \quad (9)$$

with $n_R = (\bar{n}_1 + \bar{n}_2 + 1)\cosh 2R_{12}$. In fact, for relevant case discussed below $\bar{n}_1 = 0$, we find any finite squeezing $R_{12} > 0$ yields nonzero entanglement.

From the Langevin equation Eq. (3), it is easy to verify that $\left\langle \hat{D}_i^{\text{out}}[\omega] \right\rangle$ are all zero and only 3 correlators of the output cavity modes are nonzero: $\left\langle \left(\hat{D}_1^{\text{out}}[\omega]\right)^{\dagger} \hat{D}_1^{\text{out}}[\omega] \right\rangle$, $\left\langle \left(\hat{D}_2^{\text{out}}[\omega]\right)^{\dagger} \hat{D}_2^{\text{out}}[\omega] \right\rangle$, and $\left\langle \hat{D}_1^{\text{out}}[\omega] \hat{D}_2^{\text{out}}[\omega] \right\rangle$. Thus the covariance matrix of the system is the same as a two-mode squeezed thermal state. Since two Gaussian states with the same covariance matrix represent the same state, this output cavity state can be mapped to a two-mode squeezed thermal state whose non-zero correlation function are simply

$$\left\langle \left(\hat{D}_i^{\text{out}}[\omega]\right)^{\dagger} \hat{D}_i^{\text{out}}[\omega] \right\rangle = \bar{n}_i + (\bar{n}_1 + \bar{n}_2 + 1)\sinh^2 |R_{12}[\omega]|,$$

$$\left\langle \hat{D}_1^{\text{out}}[\omega] \hat{D}_2^{\text{out}}[\omega] \right\rangle = -\frac{e^{i\theta[\omega]}}{2}(\bar{n}_1 + \bar{n}_2 + 1)\sinh 2|R_{12}[\omega]| \quad (10)$$

where $\bar{n}_i \equiv \bar{n}_i[\omega]$, $R_{12}[\omega]$ is complex in general and $\theta[\omega] \equiv \arg(R_{12}[\omega])$. Using the correlators with $\sigma = 0$ and $\omega = 0$ (i.e., output light near the cavity resonances), we find that R_{12} is real and the output state can be characterized by:

$$\bar{n}_{1,2} = \frac{\pm 2N_{\text{m}}}{C_1 - C_2 + 1} + \frac{\sqrt{E^2 - D^2} \mp 4(C_2 + N_{\text{m}})}{2(C_1 - C_2 + 1)^2} - \frac{1}{2}, \quad (11)$$

where the upper (lower) sign applies to n_1 (n_2), and

$$\tanh 2R_{12} = E/D, \quad (12)$$

where

$$D = (C_1 + C_2)^2 + 2(C_1 + C_2)(1 + 2N_{\text{m}}) + 1 + 4C_1C_2,$$
$$E = 4\sqrt{C_1C_2}(C_1 + C_2 + 1 + 2N_{\text{m}}). \quad (13)$$

Notice that such a mapping is unique, i.e., no other choice of $\bar{n}_1$, $\bar{n}_2$ and R_{12} yields the same covariance matrix. From Eqs. (9), (11) and (12), we see that the output entanglement depends only on cavity cooperativities $C_i = 4G_i^2/(\gamma\kappa_i)$ and the mechanical bath temperature (we always assume zero thermal occupancy for the two cavities).

Plugging Eqs. (11-13) into Eq. (9), one can obtain the full expression of the output entanglement including thermal effects. By focusing first on zero temperature we obtain:

$$\bar{n}_1 = 0, \qquad \bar{n}_2 = 4C_2\frac{\gamma^2}{\gamma_{\text{tot}}^2} = \frac{4C_2}{(1 + C_1 - C_2)^2}, \quad (14)$$

$$\tanh 2R_{12} = \frac{4\sqrt{C_1C_2}(C_2 + C_1 + 1)}{C_1^2 + C_2^2 + 6C_1C_2 + 2(C_1 + C_2) + 1}. \quad (15)$$

We stress that the effective thermal occupancies $\bar{n}_j$ are not simply equal to bath temperatures; in particular, $\bar{n}_2 \neq 0$ even when all input noises are vacuum. The zero-temperature output entanglement is

$$E_N^{\rm out}[0] = \ln\left(\frac{(1+C_1-C_2)^2}{A+B+2C_2\,(1+2C_1)-4\sqrt{AB}}\right), \quad (16)$$

with $A = C_2\,(C_1+C_2)$, $B = (1+C_1)^2 + C_1C_2$. Note that an analytic expression for entanglement can also be obtained at finite temperature, but it is too cumbersome to reveal much insight. In the following section, we will discuss in detail the effect of finite temperature in two different regimes. The results at both zero and finite temperature are plotted in Fig. 3.

Equations (9), (14) and (15) give us a simple way to understand entanglement generation. The ideal situation is when the two-mode squeeze parameter $R_{12} \gg 1$ and the thermal occupancy $\bar{n}_i \to 0$. From Eq. (15), we see that a large R_{12} generically requires large cooperativity. However, Eq. (14) indicates that this limit also yields a large effective temperature for cavity 2 (heuristically, $\hat{H}_{\rm int}$ turns vacuum noise into thermal noise). This heating degrades the purity of the state [31]; however, as $\bar{n}_1$ remains zero, it only slightly degrades the entanglement [26].

B. Optimal output entanglement

Equation (16) shows that the zero-temperature entanglement is only a function of C_1, C_2, thus weak-coupling does not prevent strong entanglement; for fixed C_1, the expression is optimized when

$$C_2 = C_1 + 1 \equiv C_{2,\rm opt}. \quad (17)$$

Heuristically, this condition corresponds to having a total mechanical damping $\gamma_{\rm tot} = 0$. While $E_N^{\rm out}[0]$ appears to be only a function of the C_i, the ratio κ_1/κ_2 also plays an independent role via the stability condition of Eq. (5). If $\kappa_1 \geq \kappa_2$, $C_{2,\rm opt}$ is also the maximum value of C_2 for which the system is stable. In contrast, if $\kappa_2 \geq \kappa_1$, the system becomes unstable before C_2 reaches $C_{2,\rm opt}$, hence one cannot achieve the optimal amount of entanglement. We thus see that, in addition to achieving large C_i, it is advantageous to have $\kappa_1 \geq \kappa_2$. Figure 2 illustrates the behavior of $E_N^{\rm out}[0]$ in these two cases ($C_{2,\rm opt}$ is indicated as a gray vertical line). Note that a similar dependence on κ_1/κ_2 was observed numerically in [14], but in a regime far from optimal entanglement (i.e., for $C_2 \ll C_{2,\rm opt}$).

In the large C_1 limit, the maximum achievable entanglement for the two cases reduces to:

$$E_N^{\rm out}[0]\Big|_{\rm max} \simeq \begin{cases} \ln\left(\frac{2C_1}{1+2N_{\rm m}}\right), & \kappa_1 \geq \kappa_2, \\ -\ln\left[\left(\frac{\kappa_2-\kappa_1}{\kappa_2+\kappa_1}\right)^2 + \frac{4\kappa_2^2\kappa_1 N'_{\rm m}}{C_1(\kappa_1+\kappa_2)^3}\right], & \kappa_1 < \kappa_2. \end{cases} \quad (18)$$

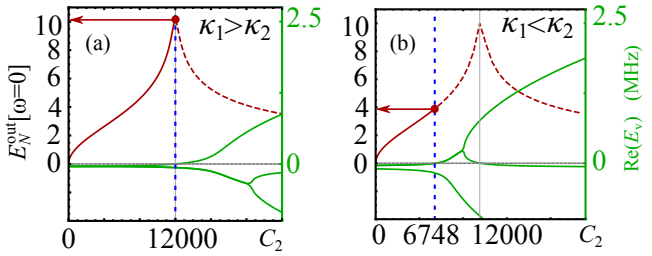

FIG. 2. Output entanglement of the two cavity fields at resonance (i.e. $\omega = 0$) as a function of C_2 for $C_1 = 12000$ in two different cases: (a) $\kappa_1 > \kappa_2$ ($\kappa_1 = 1.5\kappa_2 = 2\pi \times 0.3$ MHz), (b) $\kappa_1 < \kappa_2$ ($\kappa_1 = 0.75\kappa_2 = 2\pi \times 0.3$ MHz). Without considering the instability condition, the entanglement would reach a maximum finite value at $C_2 = C_1+1$ (gray vertical lines). The green lines show the real part of the three eigenvalues ($E_{\rm v}$) of the susceptibility matrix; the system becomes unstable when one of the real parts becomes positive, which is indicated by the blue dashed lines. The red dots indicates the maximum entanglement in each case, by also considering the stability constraints. We used $\gamma = 2\pi \times 10$ KHz. The red dashed line indicates that the system has entered the unstable regime.

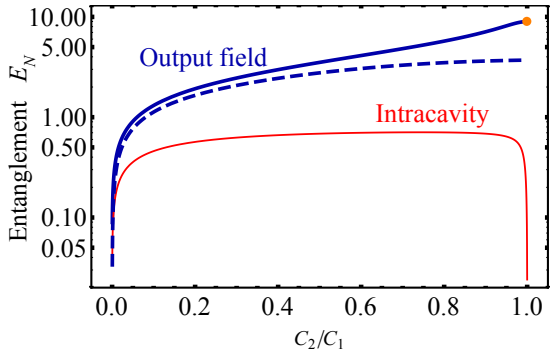

FIG. 3. Entanglement of the two cavity output fields on resonance (i.e. $\omega = 0$) (thick blue) and corresponding intracavity entanglement (thin red) as functions of C_2, with $C_1 = 4000$ and $\omega_{\rm m} \gg \kappa$ (allowing use of the RWA). The orange dot denotes the value of $\ln 2C_1$ as in Eq. (18) with $\kappa_1 \geq \kappa_2$. Except the blue dashed line (mechanical bath occupancy $N_{\rm m} = 100$), results are for zero temperature. The output E_N curves only depend on C_i. For the intracavity curve (thin red), we have also assumed strong coupling, taking $G_1 : \kappa : \gamma = 100 : 10 : 1$.

with $N'_{\rm m} = N_{\rm m}(1+\kappa_2/\kappa_1)+1$. In both cases, the output entanglement $E_N^{\rm out}$ is maximal at the boundary of system stability, similar to the behavior of a non-degenerate parametric amplifier (NDPA) [32]. However, unlike a NDPA, $E_N^{\rm out}$ does not diverge at this boundary. Further, while $E_N^{\rm out}$ is maximal at this boundary, the intra-cavity entanglement is extremely sub-optimal at this point. For $\kappa_1 \geq \kappa_2 \gg \gamma$ and $C_2 \simeq C_{2,\rm opt} \gg 1$, one has extremely large entanglement of the output fields while simultaneously having almost zero entanglement of the intracavity fields (see Fig. 3).

IV. DISCUSSION OF IMPERFECTIONS

So far we have given the analytical solution and the optimal condition for cavity output entanglement in the ideal case, where we have neglected the cavity internal loss, non-rotating wave terms, and finite bandwidth. However, for a real system there are various imperfections. We now specialize to the case $\kappa_1 = \kappa_2 = \kappa$, $C_j \gg 1$ and carefully examine the influence of various imperfections in two generic regimes.

The first is that of equal couplings $G_1 = G_2 = G$ (i.e., $C_1 = C_2$) which, as discussed, is essentially optimal for maximizing $E_N^{\rm out}[0]$ (it is also an ideal point to generate quantum-limited amplification [33]). In this regime, the effective coupling $\tilde{G}$ in Eq. (2) vanishes, meaning that the three normal modes of $\hat{H}_{\rm int}$ are degenerate. Consequently, the $\sigma = 0$ entanglement spectrum $E_N^{\rm out}[\omega]$ has a single peak at $\omega = 0$ (see thick curves in Fig. 4(a)) of width $\sim \gamma C^{3/4}$ in the weak-coupling case (red curve) and $\sim \sqrt{G}\left(2\kappa^5\gamma\right)^{1/12}$ in the strong-coupling case (green curve). We stress that achieving large optimal E_N in this regime only requires strong cooperativities, and not the more stringent strong coupling condition $G_j > \kappa_j$ (c.f. Eq. (18)).

Keeping $\kappa_1 = \kappa_2$ and $C_j \gg 1$, another generic regime is where G_2/G_1 is sufficiently smaller than 1 such that the effective coupling $\tilde{G}$ is larger than κ, γ; this necessarily requires $G_1 > \kappa$. In this regime, the three normal modes of $\hat{H}_{\rm int}$ are spectrally resolved and $E_N^{\rm out}[\omega]$ has correspondingly three peaks [14], see the thin blue curve of Fig. 4(a). The entanglement at $\omega = 0$ is necessarily much smaller than the optimal value in Eq. (18). One finds that $C_1 \gg 1$ is not by itself enough to ensure large E_N in this regime; one also needs to be deep in the strong coupling regime, $G_1 \gg \kappa$. As discussed in [14], this "resolved-modes" regime does however offer enhanced protection against mechanical thermal noise, as the central peak is due to the mechanically-dark normal mode β_B.

A. Thermal resilience of entanglement

Thermal fluctuation severely limits the coherence of the low-frequency mechanical resonator and it is important to improve the thermal resilience for protocols where the mechanics acts as a coherent mediator, such as for state transfer [34, 35]. The bipartite entanglement mediated by the mechanics also suffers from mechanical thermal noise. While the analytical solution including thermal noise has been derived in the previous section, we discuss here the thermal resilience of the output entanglement in the two representative regimes mentioned above, in order to elucidate the function of the "mechanically-dark mode" [14, 34–36].

For the first regime $G_1 = G_2 = G$ and $\kappa_1 = \kappa_2 = \kappa$ (i.e., $C_1 = C_2$), the entanglement value at $\omega = 0$ is

$$E_N^{\rm out}[0] \approx \ln\left(\frac{2C}{1+2N_{\rm m}}\right) + \mathcal{O}\left(C^{-1}\right), \qquad (19)$$

We stress that a robust peak in $E_N^{\rm out}[\omega]$ remains in the weak-coupling case $G < \kappa$ as long as $C \gg 1$.

The entanglement at $\omega = 0$ in the equal-coupling regime shows a prominent decrease with temperature due to the mechanical thermal noise. At low temperature, the equal-coupling regime ($G_1 = G_2$) yields a decent entanglement even for weak coupling ($\kappa > G$) as shown by the green curve in Fig. 4(b).

We turn now to another regime: $\tilde{G} = \sqrt{G_1^2 - G_2^2} > \kappa$, where the three normal modes of the interaction Hamil-

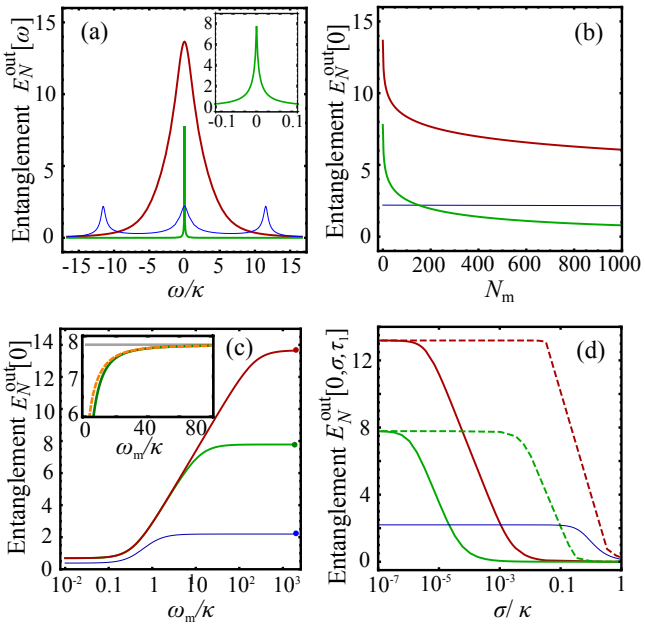

FIG. 4. (a) Output entanglement in the limit of small mode bandwidth ($\sigma \to 0$) as a function of mode center frequency ω, for 3 cases: strong equal-coupling (red thick upper line, $G_1 = G_2 = 13.3\kappa$), weak equal-coupling (green thick lower line, $G_1 = G_2 = 0.1\kappa$) and resolved normal-modes (blue thin line, $G_1/\kappa = 13.3$ and $G_2/\kappa = 6.7$. For the blue and red curves, $\gamma/\kappa = 1.67 \times 10^{-3}$ while for the green curve $\gamma/\kappa = 3.3 \times 10^{-5}$. The inset shows a zoom-in of the green curve (weak coupling case). (b) Thermal resilience. The output entanglement at $\omega = 0$ is plotted *vs.* $N_{\rm m}$ for the 3 cases. (c) The influence of counter-rotating terms. For the 3 cases, the curves show how the output entanglement $\bar{E}_N^{\rm out}[\omega = 0]$ including the counter-rotating terms approaches the RWA results neglecting those terms (marked by the dots) as $\omega_{\rm m}/\kappa$ increases. The inset shows a good fit of the analytical expression Eq. (29) (dashed lines) with the numerical result (solid line) in the weak equal-coupling case and the gray line indicates the RWA result. (d) Effects of non-zero mode bandwidth σ on the output entanglement of modes with center frequency $\omega = 0$. The solid lines are for zero time-delay between the two cavity output modes ($\tau_1 = 0$, c.f. Eq. (6)) while the dashed lines are the result including an optimal time delay $\tau_1 = \kappa/(4G^2)$.

tonian in Eq. (1) are spectrally resolved. In this regime (as discussed in [14]), $E_N^{\rm out}[\omega]$ has three resolved peaks, with each peak corresponding to a normal mode. The "dark mode" β_B corresponds to the peak at $\omega = 0$, while the peaks at $\pm\tilde{G}$ are the coupled "hybrid" modes (see blue thin curve in Fig. 4(a)); all have width $\sim \kappa$. In the simple case $\kappa_1 = \kappa_2$, resolving the normal modes requires $G_1 > \kappa \cosh r \gg \kappa$, i.e., deep in the strong coupling regime for a large r. For typical parameters, the maximum entanglement in the resolved-peaks regime is far less than the optimal value that would be achieved if C_2 were increased to C_1 (see Fig. 4(b)). On the other hand, the output entanglement at the central peak can be written as (assuming $N_{\rm m}e^{2r} \ll \tilde{C}$)

$$E_N^{\rm out}[0] \approx 4r - 2e^{2r}\left(2N_{\rm m}+1\right)/\tilde{C}, \tag{20}$$

with the effective cooperativity $\tilde{C} = 4\tilde{G}^2/\gamma\kappa$. This shows that, as the central peak corresponds to the dark mode, the mechanical noise is suppressed by the effective cooperativity and the entanglement is robust to thermal fluctuations [14] as shown in Fig. 4(b). The entanglement at the side peaks (bright modes involving the mechanics) is still sensitive to thermal noise and in the large r limit:

$$E_N^{\rm out}\left[\omega = \pm\tilde{G}\right] \approx 2r - \ln\left(\frac{4\gamma}{\kappa}\left(N_{\rm m}+\frac{1}{2}\right)\right), \tag{21}$$

valid if $\gamma N_{\rm m}/\kappa \ll 1$.

B. Influence of cavity internal losses

Except the loss through output channels, there is also extra zero-point noise incident on the cavity which can be described by the internal damping rate κ_i'. This can be treated as an additional independent input channel in the Langevin equations for the cavities. In contrast to the generation of intracavity entanglement [26], the output entanglement is sensitive to the internal losses of the cavities (cf. Eq. (3)).

a. Equal coupling case. With finite internal loss $\kappa_1' = \kappa_2' = \kappa'$ and also assuming $G \gg \gamma,\ \kappa,\ \kappa'$, the entanglement reads:

$$E_N^{\rm out}[0] \approx -\ln\left(\frac{\kappa'}{\kappa'+\kappa}+\frac{1}{2C}\right), \tag{22}$$

which recovers the two limits:

$$E_N^{\rm out}[0] \approx \ln 2C \tag{23}$$

at small internal loss ($\kappa/\kappa' \gg C \gg 1$), and

$$E_N^{\rm out}[0] \approx \ln\left(1+\kappa/\kappa'\right) \tag{24}$$

at large internal loss ($\kappa/\kappa' \ll 2C$). In the case of a cavity with tunable external damping rate, the optimal κ satisfies $\kappa = \kappa'\left(\sqrt{2C'}-1\right)$, with $C' = 4G^2/\kappa'\gamma$. The corresponding entanglement is $E_N^{\rm out}[0] \approx \frac{1}{2}\ln(C'/2)$. This result is the same as the optimal intracavity entanglement, as shown in Eq. (11) of [26] (notice that the definition of C in this paper differs by a factor of 4 compared to [26]). Thus, the maximum entanglement for both spectral entanglement and intracavity entanglement are the same.

b. Resolved peaks case. Including internal loss and assuming $\kappa_i' = \kappa'$, $\tilde{G} \gg \kappa,\ \gamma,\ \kappa'$ we have:

$$E_N^{\rm out}[0] \approx 4r - \ln\left(\frac{\kappa+e^{4r}\kappa'}{\kappa+\kappa'}+\frac{e^r\sinh r}{\tilde{C}}\right). \tag{25}$$

When $\kappa/\kappa' \ll e^{4r}\tilde{C}/(e^{2r}+\tilde{C})$, this reduces to $E_N^{\rm out}[0] \approx \ln\left(1+\kappa/\kappa'\right)$. The maximum of entanglement in Eq. (25) is obtained as follows:

$$E_{N,\rm opt}^{\rm out}[0] = 4r - \ln\left(1+\sqrt{\frac{2}{\tilde{C}}}\frac{e^{4r}-1}{\sqrt{e^{2r}+1}}+\frac{1-e^{2r}}{\tilde{C}}\right). \tag{26}$$

with

$$\kappa_{\rm opt} = \kappa'\left(\sqrt{\tilde{C}\left(1+e^{2r}\right)/2}-1\right).$$

However, notice that in order to have resolved peaks, $\tilde{G} \gg \kappa+\kappa'$. This means the optimal condition is normally not satisfied unless $\kappa' \ll \gamma$.

C. Influence of counter-rotating wave terms

So far, we only discussed the dynamics with the rotating wave approximation (RWA), considering the good cavity limit $\kappa \ll \omega_{\rm m}$. Here we will give the full result including the non-RWA terms and show that the RWA condition can be more stringent in certain regimes.

First, we notice that the counter-rotating terms are time-independent in the rotating frame with respect to the cavity drives. In this frame, the full Hamiltonian is written as $\hat{H} = \omega_{\rm m}\left(\hat{b}^\dagger\hat{b}+\hat{d}_1^\dagger\hat{d}_1-\hat{d}_2^\dagger\hat{d}_2\right)+\hat{H}_{\rm int}+\hat{H}_{\rm CR}$ with

$$\begin{aligned}\hat{H}_{\rm int} &= \left(G_1\hat{b}^\dagger\hat{d}_1+G_2\hat{b}\hat{d}_2\right)+h.c.\\ \hat{H}_{\rm CR} &= \left(G_1\hat{b}^\dagger\hat{d}_1^\dagger+G_2\hat{b}\hat{d}_2^\dagger\right)+h.c..\end{aligned} \tag{27}$$

Thus, a closed set of equations in the frequency domain can be obtained:

$$
\begin{aligned}
-i\left(\omega-\omega_{\mathrm{m}}\right)\hat{b}\left[\omega\right] &= -\frac{\gamma}{2}\hat{b}\left[\omega\right]-iG_1\left(\hat{d}_1\left[\omega\right]+\hat{d}_1^{\dagger}\left[\omega\right]\right)-iG_2\left(\hat{d}_2^{\dagger}\left[\omega\right]+\hat{d}_2\left[\omega\right]\right)-\sqrt{\gamma}\hat{b}_{in}\left[\omega\right],\\
-i\left(\omega-\omega_{\mathrm{m}}\right)\hat{d}_1\left[\omega\right] &= -\frac{\kappa_1}{2}\hat{d}_1\left[\omega\right]-iG_1\left(\hat{b}\left[\omega\right]+\hat{b}^{\dagger}\left[\omega\right]\right)-\sqrt{\kappa_1}\hat{d}_{in,1}\left[\omega\right],\\
-i\left(\omega-\omega_{\mathrm{m}}\right)\hat{d}_2^{\dagger}\left[\omega\right] &= -\frac{\kappa_2}{2}\hat{d}_2^{\dagger}\left[\omega\right]+iG_2\left(\hat{b}\left[\omega\right]+\hat{b}^{\dagger}\left[\omega\right]\right)-\sqrt{\kappa_2}\hat{d}_{in,2}^{\dagger}\left[\omega\right].
\end{aligned}
\tag{28}
$$

These equations can be solved analytically. Figure 4(c) shows the comparison of the results for $E_N^{\mathrm{out}}\left[\omega=0\right]$ with/without RWA. The lower curve corresponds to the case where $\tilde{G}>\kappa$ and the normal modes are resolved: counter-rotating terms suppress the entanglement, but become insignificant once $\omega_{\mathrm{m}}>\kappa$. The two upper curves correspond to the case with equal-coupling. In the good cavity limit, the maximum entanglement in the equal-coupling regime is much larger than the resolved-peak regime. Consequently, non-RWA corrections play a larger role, and one can only achieve the RWA result deep into the good cavity limit $\omega_{\mathrm{m}}\gg\kappa$.

For both equal-coupling and resolved-peak cases, the leading non-RWA correction to $E_N^{\mathrm{out}}\left[0\right]$ is

$$
\bar{E}_N^{\mathrm{out}}\left[0\right]-E_N^{\mathrm{out}}\left[0\right]\approx -e^{E_N^{\mathrm{out}}[0]}\frac{\kappa^2}{16\omega_{\mathrm{m}}^2}. \tag{29}
$$

Here $\bar{E}_N^{\mathrm{out}}\left[0\right]$ is the entanglement including the counter-rotating terms. This approximate expression is shown by the orange dashed line in the inset of Fig. 4(c). Thus the condition to justify the use of RWA is

$$
\left|\frac{\omega_{\mathrm{m}}}{\kappa}\right|\gg\frac{1}{4}\sqrt{\frac{e^{E_N^{\mathrm{out}}}}{E_N^{\mathrm{out}}}}, \tag{30}
$$

which is looser in the case of resolved-peaks (due to the smaller E_N^{out}).

D. Time delay to improve the entanglement bandwidth

So far, we have considered the output entanglement with zero bandwidth, i.e., $E_N^{\mathrm{out}}[\omega,\sigma=0,\tau_1]$. However, in practice, the filter function has a finite bandwidth. Assuming the center frequency is set at $\omega=0$ (the cavity resonance frequency in the lab frame), the entanglement has a non-trivial dependence on the bandwidth σ and the relative time delay τ_1 (taking $\tau_2=0$).

The solid lines of Fig. 4(d) show the entanglement of the two output cavity modes for zero time delay $E_N^{\mathrm{out}}[\omega=0,\sigma,\tau_1=0]$ as a function of bandwidth σ. While the equal-coupling case yields large entanglement at $\sigma=0$, it is much more sensitive to the increase of the bandwidth. $E_N^{\mathrm{out}}[0,\sigma,0]$ decays on a scale $\sigma\sim C^{-1/4}\gamma$. In contrast, in the resolved normal-mode case, $E_N^{\mathrm{out}}[0,\sigma,0]$ is less sensitive to increasing the mode bandwidth, and is only suppressed significantly when $\sigma\sim\kappa$.

The strong sensitivity to non-zero σ in the case of equal-coupling is related to the change of squeezing phase

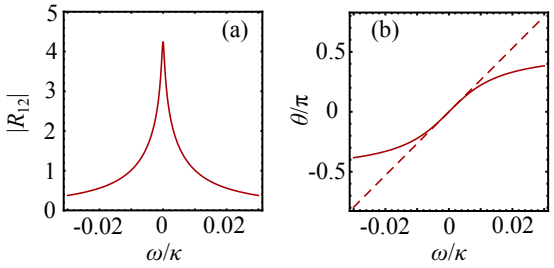

FIG. 5. The dependence of the squeezing parameter $R_{12}[\omega]=|R_{12}|e^{i\theta}$ on frequency. The left panel shows the magnitude change of R_{12}, while the right panel shows the phase change of R_{12}. The dashed line in the right panel is the linear dependence given by Eq. (31). The parameters used are $G/\kappa=0.1$, $\gamma/\kappa=3.3\times10^{-5}$.

at different ω. As discussed before, the cavity output state can be characterized by a 2-mode squeezed thermal state (see Eq. (7)) with a complex squeezing parameter $R_{12}\left[\omega\right]$ whose phase is $\theta\left[\omega\right]=\arg\left\langle-\hat{D}_1^{\mathrm{out}}\left[\omega\right]\hat{D}_2^{\mathrm{out}}\left[\omega\right]\right\rangle$, (see Eq. (10)). At $\omega=0$ and $\sigma=0$, $R_{12}\left[0\right]$ is real (see Eq. (15)), i.e., $\theta=0$. For $\omega\neq0$, a frequency-dependent phase arises (see Fig. 5(b)). In the large squeezing limit, i.e., $|R_{12}|\gg1$, such a phase variation leads to a rapid decrease of entanglement as σ increases. Assuming $\kappa_1=\kappa_2$ and $G_1=G_2$, where the magnitude of squeezing is maximized, the peak width of $|R_{12}|[\omega]$ is comparable to that of $E_N^{\mathrm{out}}[\omega]$. The corresponding phase variation is approximately linear in the vicinity of $\omega=0$ (as shown by the dashed line in Fig. 5(b))

$$
\delta\theta\approx(\kappa/4G^2)\delta\omega. \tag{31}
$$

This suggests (as per Eq. (6)), that the optimal entanglement is between a cavity-2 mode emitted at $\tau_2=0$ and a cavity-1 mode emitted at $\tau_1=\kappa/4G^2$. The entanglement with time delay is shown by the red-dashed curve in Fig. 4(d). On a heuristic level, one could think that our system first generates entangled phonon - cavity 2 photon pairs via the G_2 interaction in Eq. (2); next the G_1 interaction swaps the phonon state into a photon in cavity 1. This physical picture is in agreement with finding that the optimal entanglement involves a positive delay for the cavity 1 output mode, as in Fig. 4(d). Finally, we note that for ω away from 0, the squeezing phase θ has a nonlinear frequency dependence, and hence the optimal filter function for larger σ will not correspond to a simple delay as in Eq. (31).

V. GENUINE TRIPARTITE ENTANGLEMENT OF THE ITINERANT MODES

As mentioned in the introduction, alternative methods exist to access the mechanical output field. We discuss them in detail below and, motivated by these possibilities, we analyze the multipartite entanglement properties of all three output fields in our system. Note that previous work studied the non-stationary tripartite entanglement of intracavity fields generated by the *closed-system* Hamiltonian $\hat{H}_{\rm int}$ in Eq. (2) [37]; in contrast, our focus here is on the steady-state output entanglement in our *dissipative* 3-mode system.

A. Phonon output through an auxiliary cavity

Experimental setups using optomechanical crystals [20, 38] could access the mechanical output field via engineered phonon waveguides. For a general optomechanical system where a phonon waveguide is absent, we find it is still possible to access the phonon output by having its damping dominated by the optical damping of an auxiliary cooling cavity (see Fig. 1). This auxiliary cavity will have a large damping rate, and will be coupled to the mechanics via a linearized optomechanical coupling (the cavity is strongly driven by a red-detuned laser):

$$\hat{H}_{\rm a} = G_{\rm a}\left(\hat{b}\hat{d}_{\rm a}^{\dagger} + \hat{b}^{\dagger}\hat{d}_{\rm a}\right), \tag{32}$$

where $\hat{d}_{\rm a}$ is the annihilation operator of the auxiliary cavity and $G_{\rm a}$ is the corresponding coupling. The auxiliary cavity, due to the large damping rate $\kappa_{\rm a}$, can be described by the following steady-state relation:

$$\hat{d}_{\rm a} = -i\frac{2G_{\rm a}}{\kappa_{\rm a}}\hat{b} - \frac{2}{\sqrt{\kappa_{\rm a}}}\hat{d}_{\rm a}^{\rm in}. \tag{33}$$

Plugging this into the equation of motion for the mechanical resonator one obtains

$$\frac{d}{dt}\hat{b} = -\frac{2G_{\rm a}^2}{\kappa_{\rm a}}\hat{b} - i\left(G_1\hat{d}_1 + G_2\hat{d}_2^{\dagger}\right) + \frac{2iG_{\rm a}}{\sqrt{\kappa_{\rm a}}}\hat{d}_{\rm a}^{\rm in}, \tag{34}$$

where we have neglected other damping channels of the resonator, supposing that $G_{\rm a}^2/\kappa_{\rm a}$ is sufficiently large. Comparing Eq. (34) with the Langevin equation without an auxiliary cavity, $\frac{d}{dt}\hat{b} = -\frac{\gamma}{2}\hat{b} - i\left(G_1\hat{d}_1 + G_2\hat{d}_2^{\dagger}\right) - \sqrt{\gamma}\hat{d}_{\rm a}^{\rm in}$, we can identify

$$\hat{b}^{\rm in} = -i\hat{d}_{\rm a}^{\rm in}, \text{ and } \gamma = 4G_{\rm a}^2/\kappa_{\rm a}. \tag{35}$$

The input-output relation of the auxiliary cavity is $\hat{d}_{\rm a}^{\rm out} = \hat{d}_{\rm a}^{\rm in} + \sqrt{\kappa_{\rm a}}\hat{d}_{\rm a}$ which, together with Eqs. (33) and (35), gives $\hat{d}_{\rm a}^{\rm out} = -i\sqrt{\gamma}\hat{b} - i\hat{b}^{\rm in}$, thus

$$\hat{d}_{\rm a}^{\rm out} = -i\hat{b}^{\rm out}. \tag{36}$$

This shows that a strongly damped auxiliary cavity can serve as output of the mechanical mode.

B. 3-mode output state

We focus on zero frequency and zero bandwidth, and consider the ideal case where all dissipative baths are at zero temperature. In this case, the 3-mode output state is a pure state $|\Psi_s\rangle$. Since $\bar{n}_1 = 0$ (see Eq. (14)), cavity 1 must be in the ground state if we consider the "unsqueezed" state $|\Psi_s\rangle \equiv \tilde{S}_{12}(-R_{12})|\Psi\rangle$. However, $|\Psi_s\rangle$ has residual entanglement between cavity 2 and the mechanical mode. This is clear from the finite value of $\bar{n}_2$, which diverges at the instability condition $\gamma_{\rm tot} = 0$ (the finite population $\bar{n}_2$ is a consequence of tracing out the mechanical mode). One can compute explicitly the correlations of the state $|\Psi_s\rangle$ and identify it as a squeezed vacuum of cavity 2 and the mechanical mode, with squeezing parameter $R_{2\rm m} = \sinh^{-1}\bar{n}_2$. Hence the output state can be written as a twice-squeezed vacuum

$$|\Psi\rangle = \hat{S}_{12}(R_{12})\,\hat{S}_{2\rm m}(R_{2\rm m})\,|000\rangle, \tag{37}$$

where $\hat{S}_{2\rm m}(R_{2\rm m}) \equiv \exp\left[iR_{2\rm m}\hat{D}_{\rm m}^{\rm out}[0]\,\hat{D}_2^{\rm out}[0] - h.c.\right]$ is the 2-mode squeeze operator entangling the output of the mechanics at $\omega = 0$ (denoted by $\hat{D}_{\rm m}^{\rm out}[0]$, which is defined in a similar way as the cavity output) with that of cavity 2. Since the effective temperature represented by $\bar{n}_2$ diverges at the instability point (see Eq. (14)), the squeezing parameter $R_{2\rm m} = \sinh^{-1}\bar{n}_2$ diverges as well. Equation (37) demonstrates that the effective temperature $\bar{n}_2$ which degraded the cavity-cavity entanglement in Eq. (14) is a direct consequence of entanglement between cavity 2 and the mechanics. It also demonstrates the asymmetry between the three modes (i.e., there is no direct squeezing between the mechanical and cavity 1 outputs).

Furthermore, Eq. (37) shows that we have genuine tripartite entanglement (GTE): none of the parties can be separated from any other in a mixture of product states, implying a fully inseparable state [39, 40]. To see this, note that the total state is pure, and if one traces over one subsystem, the remaining two are in a mixed state. GTE is also evident by writing the state in the Fock-state basis $|n_1, n_2, n_{\rm m}\rangle$,

$$|\Psi\rangle = \sum_{pq}\frac{\sqrt{C_{p+q}^{p}}\,\langle N_{\rm m}\rangle^{\frac{q}{2}}\,\langle N_1\rangle^{\frac{p}{2}}}{\left(1+\langle N_2\rangle\right)^{(p+q+1)/2}}\,|p, p+q, q\rangle, \tag{38}$$

where C_{p+q}^{p} are binomial coefficients and $\langle N_i\rangle = \left\langle\left(\hat{D}_i^{\rm out}[0]\right)^{\dagger}\hat{D}_i^{\rm out}[0]\right\rangle$ $(i = 1, 2, {\rm m})$ is the average photon/phonon number of each mode

$$\begin{aligned}\left\langle\hat{N}_1\right\rangle &= \frac{4C_1C_2}{\left(1+C_1-C_2\right)^2},\\ \left\langle\hat{N}_2\right\rangle &= \frac{4C_2\left(C_1+1\right)}{\left(1+C_1-C_2\right)^2},\\ \left\langle\hat{N}_{\rm m}\right\rangle &= \frac{4C_2}{\left(1+C_1-C_2\right)^2}.\end{aligned} \tag{39}$$

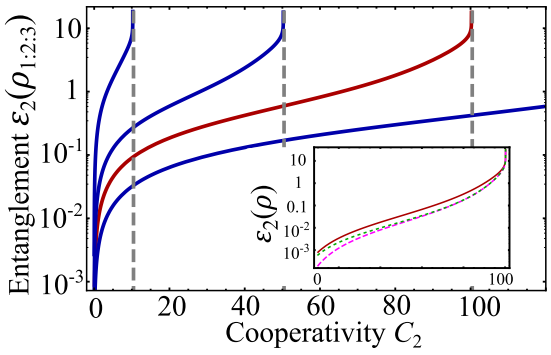

FIG. 6. 3-mode entanglement, evaluated by the residual GR2 entanglement with cavity-1 as the focus mode $\epsilon_2(\rho_{1:2:3})$, versus the cooperativity of cavity 2. Here C_1 is fixed to 10, 50, 100, 200 (from top to bottom). The gray dashed lines indicate the onset of system instability. The 3-mode entanglement diverges at $\gamma_{\rm tot}=0$ or $C_2=C_1+1$. The $C_1=100$ (red) curve is re-plotted in the inset, together with the two residual GR2 entanglement where the focus mode is cavity-2 ($\epsilon_2(\rho_{2:1:3})$) or mechanics ($\epsilon_2(\rho_{3:2:1})$).

$|\Psi\rangle$ only involves Fock states $|n_1,n_2,n_{\rm m}\rangle$ where $n_2=n_1+n_{\rm m}$; there is thus a perfect correlation between the three systems that is only evident by looking at all three modes. If any two modes are traced out, the remaining third mode is in an impure thermal state. Another interesting observation is that, although the tripartite steady state Eq. (37) is generated by interaction between intracavity modes and the input-output relations, the output state described by Eq. (37) could also be achieved by a unitary evolution generated by the following interaction between the output modes:

$$\begin{aligned}\tilde{H}=&R_{12}\sin R_{2{\rm m}}\hat{D}_{\rm m}^{\rm out}[0]\,\hat{D}_2^{\rm out}[0]-R_{2{\rm m}}\left(\hat{D}_{\rm m}^{\rm out}[0]\right)^{\dagger}\hat{D}_1^{\rm out}[0]\\&+iR_{12}\cos R_{2{\rm m}}\hat{D}_1^{\rm out}[0]\,\hat{D}_2^{\rm out}[0]+h.c.\end{aligned}\tag{40}$$

This result can be obtained by Wei-Norman decomposition in terms of a closed algebra $\{\hat{D}_{\rm m}^{\rm out}[0]^{\dagger}\hat{D}_1^{\rm out}[0]+h.c.,\hat{D}_{\rm m}^{\rm out}[0]\,\hat{D}_1^{\rm out}[0]+h.c.,\hat{D}_1^{\rm out}[0]\,\hat{D}_2^{\rm out}[0]-h.c.\}$.

C. 3-mode entanglement measure based on Rényi-2 Entropy

The tripartite entanglement can be measured by the residual Gaussian Rényi-2 (GR2) entanglement [21]. We find that it is indeed non-zero, and diverges as one increases C_2 to the instability point C_1+1 (due to the divergence of $\bar{n}_2$ and $R_{2{\rm m}}$). These calculations also reveal the absence of any direct entanglement between the mechanical and cavity 1 outputs.

The Rényi-2 entropy is given by $S_2(\rho)=-\ln{\rm Tr}\left(\rho^2\right)$ and allows to define an entanglement measure $\varepsilon_2(\rho_{A:B})$ for bipartite states ρ_{AB}. For pure states one simply has $\varepsilon_2(\rho_{A:B})=S_2(\rho_A)$, with ρ_A the reduced density matrix of subsystem A. The tripartite entanglement is then characterized through the residual entanglement $\varepsilon_2(\rho_{i:j:k})$, given by:

$$\varepsilon_2(\rho_{i:j:k})=\varepsilon_2(\rho_{i:jk})-\varepsilon_2(\rho_{i:k})-\varepsilon_2(\rho_{i:j})\geq 0,\tag{41}$$

where $i\neq j\neq k=1,2,3$ represent the 3 different modes (the 3rd mode denotes the mechanics in our case). In Eq. (41), $\varepsilon_2(\rho_{i:jk})$ is the bipartite entanglement partitioning the global system into $A=i$ and $B=jk$, while $\varepsilon_2(\rho_{i:j})$ and $\varepsilon_2(\rho_{i:k})$ consider the reduced density matrices of subsystems ij and ik, respectively. In general, three different values of $\varepsilon_2(\rho_{i:j:k})$ are obtained, depending on the choice of the "focus mode" i. There are special cases when $\varepsilon_2(\rho_{i:j:k})$ is invariant under mode permutation [21]; as we explain below, that is not the case for our system.

For pure tripartite Gaussian states, $\varepsilon_2(\rho_{i:j:k})$ can be evaluated analytically [21]. The first term of Eq. (41) is:

$$\varepsilon_2(\rho_{i:jk})=S_2(\rho_i)=\ln a_i,\tag{42}$$

where a_i is related to the covariance matrix $\mathbf{V}_i$ of subsystem i:

$$a_i=\sqrt{\det\mathbf{V}_i}.\tag{43}$$

Using the covariance matrix for our system, calculated from the Langevin equation, it is possible to obtain explicit formulas for $\varepsilon_2(\rho_{1:23})$, $\varepsilon_2(\rho_{2:13})$, $\varepsilon_2(\rho_{3:12})$ in terms of the cooperativities $C_{1,2}$. Although we omit them here, it is worth mentioning that these three quantities are all non-zero, showing that none of the three systems is separable.

The last two terms in Eq. (41) are given by [21]:

$$\varepsilon_2(\rho_{j:k})=\frac{1}{2}\ln g_i\quad(i\neq j\neq k),$$

where

$$g_i=\begin{cases}1, & a_k\geq\sqrt{a_i^2+a_j^2-1},\\ \frac{\beta}{8a_k^2}, & \alpha_k<a_k<\sqrt{a_i^2+a_j^2-1},\\ \left(\frac{a_i^2-a_j^2}{a_k^2-1}\right)^2 & a_k\leq\alpha_k,\end{cases}\tag{44}$$

with

$$\alpha_k = \sqrt{\frac{2\left(a_i^2+a_j^2\right)+\left(a_i^2-a_j^2\right)^2+\left|a_i^2-a_j^2\right|\sqrt{\left(a_i^2-a_j^2\right)^2+8\left(a_i^2+a_j^2\right)}}{2\left(a_i^2+a_j^2\right)}},$$
$$\beta = 2a_1^2+2a_2^2+2a_3^2+2a_1^2a_3^2+2a_2^2a_3^2+2a_1^2a_2^2-a_1^4-a_2^4-a_3^4-\sqrt{\delta}-1,$$
$$\delta = \left(\left(a_1-a_2-a_3\right)^2-1\right)\left(\left(a_1+a_2-a_3\right)^2-1\right)\left(\left(a_1-a_2+a_3\right)^2-1\right)\left(\left(a_1+a_2+a_3\right)^2-1\right).$$

Since $\varepsilon_2(\rho_{j:k})$ is the GR2 2-mode entanglement measure in the subspace where the mode i is eliminated, it serves as an alternative way to quantify the 2-mode entanglement in our system, other than the logarithmic negativity used in Sec. III. We obtain all the two-mode entanglements as follows:

$$\begin{aligned}
\varepsilon_2(\rho_{1:2}) &= \ln\frac{(1+C_2)^2+C_1^2+2C_1+6C_1C_2}{(1+C_2)^2+C_1^2+2C_1-2C_1C_2} \approx \ln\frac{C_2^2+6C_1C_2+C_1^2}{(C_1-C_2)^2}+\mathcal{O}\left(\frac{1}{C_2}\right),\\
\varepsilon_2(\rho_{3:2}) &= \ln\frac{(1+C_1)^2+C_2^2+6C_2+2C_1C_2}{(1-C_2)^2+C_1^2+2C_1+2C_1C_2} \approx \mathcal{O}\left(\frac{1}{C_2}\right),\\
\varepsilon_2(\rho_{1:3}) &= 0,
\end{aligned} \tag{45}$$

where the last approximation is in the large C limit. These results show that the entanglement between cavity 1 and the mechanics is always zero, although the mechanics is entangled with the composite system of the two cavities ($\varepsilon_2(\rho_{3:12}) \neq 0$). In particular, there is entanglement between the mechanics and cavity 2, although it is much smaller than the entanglement between cavity 1 and 2. These results are all in agreement with those based on the logarithmic negativity.

We now turn to the evaluation of the tripartite entanglement $\varepsilon_2(\rho_{i:j:k})$, which is permutationally invariant only when all the $\varepsilon_2(\rho_{i:jk})$ and $\varepsilon_2(\rho_{i:j})$ are non-zero [21]. The fact that $\varepsilon_2(\rho_{1:3})=0$ implies that $\varepsilon_2(\rho_{i:j:k})$ depends on the focus mode, thus we consider all three choices $i=1,2,3$. Using the results for $\varepsilon_2(\rho_{i:jk})$, $\varepsilon_2(\rho_{i:j})$ discussed above, Eq. (41) gives:

$$\begin{aligned}
\varepsilon_2(\rho_{1:2:3}) &= \ln\left(\frac{C_1^2+(1+C_2)^2+2C_1-2C_1C_2}{(1+C_1-C_2)^2}\right)-2\tanh^{-1}\left(\frac{2C_2}{(1+C_1)^2+6C_1C_2+C_2^2}\right),\\
\varepsilon_2(\rho_{2:1:3}) &= \ln\left(\frac{C_2^2+(1+C_1)^2+6C_2(1+C_1)}{C_2^2+(1+C_1)^2+2C_2(3+C_1)}\right)\\
&\quad+\ln\left(\frac{\left(C_1^2+(1+C_2)^2-2C_1(C_2-1)\right)\left(C_1^2+(1-C_2)^2+2C_1(1+C_2)\right)}{(1+C_1-C_2)^2\left(C_1^2+(1+C_2)^2+2C_1(1+3C_2)\right)}\right),\\
\varepsilon_2(\rho_{3:1:2}) &= \ln\left(\frac{C_2^2+(1+C_1)^2+6C_2-2C_1C_2}{(1+C_1-C_2)^2}\right)-2\tanh^{-1}\left(\frac{4C_2}{(1+C_1-C_2)^2}\right).
\end{aligned} \tag{46}$$

As announced, the three "residual GR2 entanglements" are unequal. Nevertheless, they are all larger than zero, which confirms the presence of genuine tripartite entanglement. Furthermore, as shown in Fig. 6, the $\varepsilon_2(\rho_{i:j:k})$ all diverge at the instability point $\gamma_{\rm tot}=0$. This divergence is similar to the case of a parametric amplifier and is related to the divergences of $\bar{n}_2$ and $R_{2\rm m}$ discussed in the previous subsection.

VI. CONCLUSION

We have studied in detail the bipartite and tripartite entanglement of the output fields in a 3-mode op-

tomechanical system. For bipartite photonic entanglement, we have found an explicit analytical expression based on identifying the output with a squeezed thermal state. This has allowed us to find an optimal "impedance matching" condition for entanglement generation: tuning the system parameters to achieve this condition yields a dramatic increase of the maximum output entanglement. Strikingly, our optimal condition corresponds to a regime where entanglement between the two optical cavities is nearly zero [26], but at the same time strongly entangled photons are emitted into the output channels.

We also show that large values of the output entanglement can be achieved even in the standard "weak-coupling" regime with large cooperativity (the same regime used for cavity cooling in numerous experiments): one simply needs to tune parameters to achieve the aforementioned impedance matching condition. Furthermore, we have considered realistic conditions including different types of imperfections: finite temperature, internal losses, sizable counter-rotating terms, as well as finite mode bandwidth. By restricting ourselves to the optimal equal coupling regime, we find that it is crucial to consider time delays of emitted wave packets; we find the optimal value of this delay and show that it substantially improves the attainable entanglement. At last, we show how to generate genuine tripartite entanglement of spatially separated, itinerant quanta: we provide a simple analytic characterization of the output state and use a rigorous entanglement monotone to quantify the three-mode entanglement. Our results can also be applied to other parametrically coupled 3-mode bosonic systems, besides optomechanical systems.

We thank M. Woolley for useful discussions. This work was supported by the DARPA ORCHID program under a grant from the AFOSR. SC and YDW acknowledge support from Chinese Youth 1000 Talents Program.

[1] T. Aoki, N. Takei, H. Yonezawa, K. Wakui, T. Hiraoka, A. Furusawa, and P. van Loock, Phys. Rev. Lett. **91**, 080404 (2003).
[2] J.-W. Pan, Z.-B. Chen, C.-Y. Lu, H. Weinfurter, A. Zeilinger, and M. Żukowski, Rev. Mod. Phys. **84**, 777 (2012).
[3] J. Raimond, M. Brune, and S. Haroche, Rev. Mod. Phys. **73**, 565 (2001).
[4] M. Neeley, R. C. Bialczak, M. Lenander, E. Lucero, M. Mariantoni, D. Sank, H. Wang, M. Weides, J. Wenner, Y. Yin, T. Yamamoto, A. N. Cleland, and J. M. Martinis, Nature **467**, 570 (2010).
[5] L. DiCarlo, M. Reed, L. Sun, B. L. Johnson, J. M. Chow, J. M. Gambetta, L. Frunzio, S. M. Girvin, M. H. Devoret, and R. J. Schoelkopf, Nature **467**, 574 (2010).
[6] E. Flurin, N. Roch, F. Mallet, M. H. Devoret, and B. Huard, Phys. Rev. Lett. **109**, 183901 (2012).
[7] H. Bernien, B. Hensen, W. Pfaff, G. Koolstra, M. S. Blok, L. Robledo, T. H. Taminiau, M. Markham, D. J. Twitchen, L. Childress, and R. Hanson, Nature **497**, 86 (2013).
[8] M. Aspelmeyer, T. J. Kippenberg, and F. Marquardt, arXiv:1303.0733 (2013).
[9] M. Paternostro, D. Vitali, S. Gigan, M. Kim, C. Brukner, J. Eisert, and M. Aspelmeyer, Phys. Rev. Lett. **99**, 250401 (2007).
[10] C. Genes, A. Mari, P. Tombesi, and D. Vitali, Phys. Rev. A **78**, 032316 (2008).
[11] C. Wipf, T. Corbitt, Y. Chen, and N. Mavalvala, New J. Phys. **10**, 095017 (2008).
[12] S. G. Hofer, W. Wieczorek, M. Aspelmeyer, and K. Hammerer, Phys. Rev. A **84**, 052327 (2011).
[13] S. Barzanjeh, M. Abdi, G. Milburn, P. Tombesi, and D. Vitali, Phys. Rev. Lett. **109**, 130503 (2012).
[14] L. Tian, Phys. Rev. Lett. **110**, 233602 (2013).
[15] M. C. Kuzyk, S. J. van Enk, and H. Wang, Phys. Rev. A **88**, 062341 (2013).
[16] T. A. Palomaki, J. D. Teufel, R. W. Simmonds, and K. W. Lehnert, Science **342**, 710 (2013).
[17] C. Dong, V. Fiore, M. C. Kuzyk, and H. Wang, Science **338**, 1609 (2012).
[18] J. T. Hill, A. H. Safavi-Naeini, J. Chan, and O. Painter, Nat. Commun. **3**, 1196 (2012).
[19] R. Andrews, R. W. Peterson, T. P. Purdy, K. Cicak, R. W. Simmonds, C. A. Regal, and K. W. Lehnert, Nat. Phys. **10**, 321 (2014).
[20] A. H. Safavi-Naeini and O. Painter, New J. Phys. **13**, 013017 (2011).
[21] G. Adesso, D. Girolami, and A. Serafini, Phys. Rev. Lett. **109**, 190502 (2012).
[22] S. Braunstein and P. van Loock, Rev. Mod. Phys. **77**, 513 (2005).
[23] S. Koike, H. Takahashi, H. Yonezawa, N. Takei, S. L. Braunstein, T. Aoki, and A. Furusawa, Phys. Rev. Lett. **96**, 060504 (2006).
[24] N. Bergeal, R. Vijay, V. E. Manucharyan, I. Siddiqi, R. J. Schoelkopf, and M. Devoret, Nature Phys. **6**, 296 (2010).
[25] Baust, A. et. al., arXiv:1405.1969.
[26] Y.-D. Wang and A. A. Clerk, Phys. Rev. Lett. **110**, 253601 (2013).
[27] C. Gardiner and P. Zoller, *Quantum Noise*, 3rd ed. (Springer, New York, 2004).
[28] E. X. DeJesus and C. Kaufman, Phys. Rev. A **35**, 5288 (1987).
[29] G. Vidal and R. F. Werner, Phys. Rev. A **65**, 032314 (2002).
[30] M. B. Plenio, Phys. Rev. Lett. **95**, 090503 (2005).
[31] M. J. Woolley and A. A. Clerk, Phys. Rev. A **89**, 063805 (2014).
[32] D. F. Walls and G. J. Milburn, *Quantum optics* (Springer, Berlin, 1994).
[33] A. Metelmann and A. A. Clerk, Phys. Rev. Lett. **112**, 133904 (2014).
[34] Y.-D. Wang and A. A. Clerk, Phys. Rev. Lett. **108**, 153603 (2012).
[35] Y.-D. Wang and A. A. Clerk, New Journal of Physics **14**, 105010 (2012).
[36] L. Tian, Phys. Rev. Lett. **108**, 153604 (2012).
[37] A. Ferraro, M. G. A. Paris, M. Bondani, A. Allevi, E. Puddu, and A. Andreoni, J. Opt. Soc. Am. B **21**,

1241 (2004).
[38] M. Eichenfield, J. Chan, R. M. Camacho, K. J. Vahala, and O. Painter, Nature **461**, 78 (2009).
[39] G. Giedke, B. Kraus, M. Lewenstein, and J. I. Cirac, Phys. Rev. A **64**, 052303 (2001).
[40] P. van Loock and S. L. Braunstein, Phys. Rev. Lett. **84**, 3482 (2000).